Supplement of

Highly time-resolved chemical characteristics and aging process of submicron aerosols over the central Himalayas

Yishen Wang[1], Yanqing An[2], Yulong Tan[2], Kemei Li[2], Jianzhong Xu[1], Shugui Hou[1]

[1]School of Oceanography, Shanghai Jiao Tong University, Shanghai, 200030, China
[2]Northwest Institute of Eco-Environment and Resources, Chinese Academy of Sciences, Lanzhou 730000, China

Correspondence to: Jianzhong Xu (jzxu78@sjtu.edu.cn)

1 **Text**

2 **Text S1 HR-ToF-AMS operation**

3 A PM$_{2.5}$ cyclone was installed before the sampling line to remove coarse particles. A Nafion dryer was then used to keep the

4 relative humidity of aerosol particles below 30 % before sampling into the HR-ToF-AMS. Ambient particles are sampled

5 into the instrument through a critical orifice and focused into a concentrated and narrow beam through an aerodynamic lens.

6 Particles are then accelerated into the sizing vacuum chamber and obtain different velocities for particles with different sizes

7 due to the supersonic expansion induced by a pressure difference between the two chambers. Meanwhile, a mechanical

8 chopper with two radial slits located 180° apart is used to intercept the focused particle, and then the time of flight (P-ToF)

9 from the chopper to the vaporizer is measured to obtain the aerodynamic size of particles. After passing through the sizing

10 chamber, particles are directed onto a resistively heated surface (600 °C) under a high vacuum and ionized by a 70 eV

11 electron impact, before finally being detected by a high-resolution mass spectrometer. There are two different operation

12 modes in HR-ToF-AMS, i.e., V-mode (detection limits of about 10 ng m^{-3}) and W-mode (~5000 m/Δm) with different

13 signal-to-noise ratio (S/N). In this study, we only used V-mode in consideration of the relatively low aerosol mass

14 concentration level and low S/N ratio over the TP.

16 **Text S2 Calculation and evaluation of the acidity of submicron aerosols**

17 Bulk acidity of PM_1 was generally evaluated following the methods in Zhang et al. (2007) and Schueneman et al. (2021).

18 The mass concentration of ammonium was predicted by assuming to fully neutralize these HR-ToF-AMS measured sulfate,

19 nitrate, and chloride using the following equation:

20
$$\text{Predicted ammonium} = 18 \times \left(\frac{2 \times SO_4^{2-}}{96} + \frac{NO_3^-}{62} + \frac{Cl^-}{35.5} \right) \tag{S1}$$

21 The mass concentration ratio of measured ammonium to predicted ammonium can be further calculated to be an indicator to

22 evaluate the bulk acidity of submicron aerosols. In this study, linear regression analysis between the mass concentrations of

23 measured and predicted ammonium was performed to evaluate the bulk acidity of submicron aerosols (Fig. S2). Aerosol

24 particles are generally considered to be "acidic" if the calculated ratio is obviously lower than 1 and to be "more acidic" if

25 the ratio is lower than 0.75, whereas a ratio that roughly near to 1 or larger than 1 indicates the particles are "bulk

26 neutralized" and even there are more excess ammonium that needed to be neutralized. Note that the validity of using this

27 method is based on the assumption that the influence from nitrogen- or sulfur-containing organic ions (e.g., organic acids

28 and organic nitrogen compounds) as well as the mineral and metal ions are negligible (Zhang et al., 2007).

29

30 **Text S3 The box model description**

31 Based on the box model described in Chen et al. (2021), the formation rate of species i is given by:

32
$$\frac{dc_i}{dt} = \frac{Q_i}{H(t)} + R_i - \frac{v_{d_i} c_i}{H(t)} + \frac{u}{\Delta x}\left(c_i^0 - c_i\right) + \frac{1}{H(t)}\frac{dH}{dt}\bigg|_{dH/dt>0}\left(c_i^a - c_i\right) \qquad (S2)$$

33 where $H(t)$ is the ABLH, Q_i is the emission rate, R_i is the chemical production and loss rate, v_{d_i} is the deposition velocity, c_i^0

34 is the background concentration of species i, c_i^a is the aloft concentration of species i, and u is the wind speed (with a

35 constant Δx direction).

36
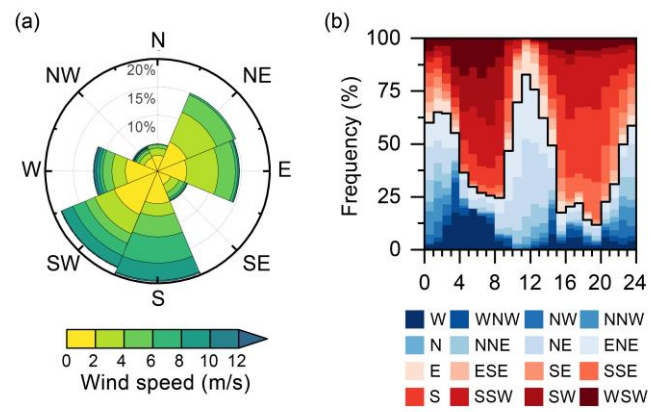
37   **Figures**

38

39   **Figure S1. (a)** The wind rose plot colored by wind speed during the field study period and **(b)** the diurnal variation of wind
40   direction.

41
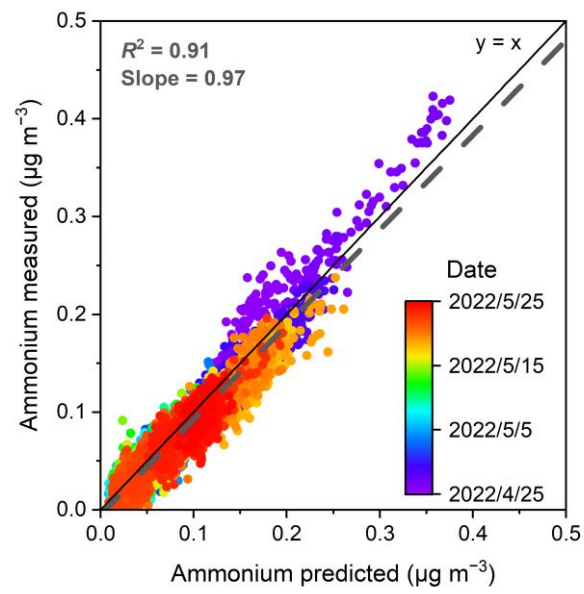
42

43 **Figure S2.** Scatterplot and linear regression (grey dashed line) of measured ammonium versus predicted ammonium.

44
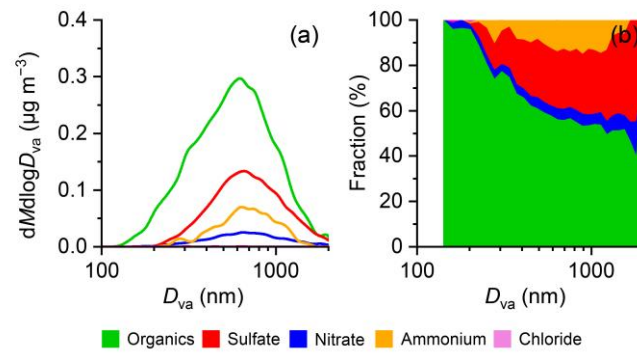
45

46 **Figure S3. (a)** Averaged mass size distributions of NR-PM$_1$ and **(b)** the fraction of species as a function of particle sizes.

47
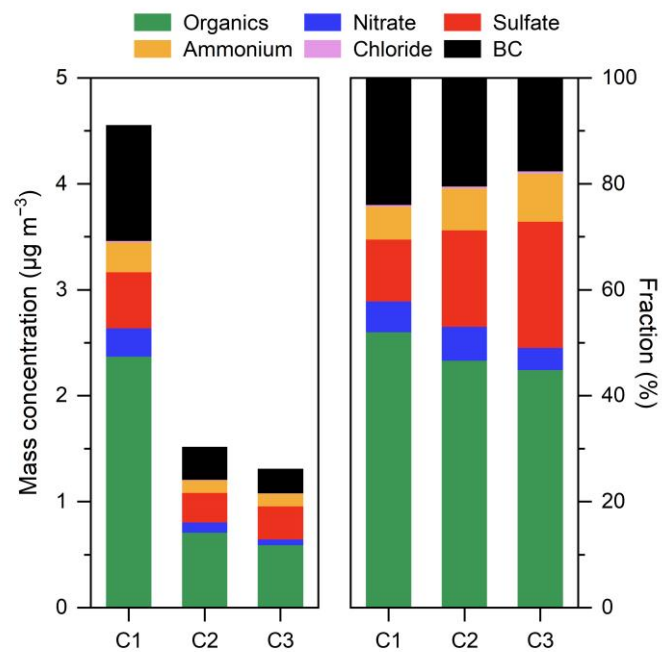
48

49 **Figure S4.** The PM$_1$ mass concentration and fraction of each trajectory cluster during polluted period and clean period.

50
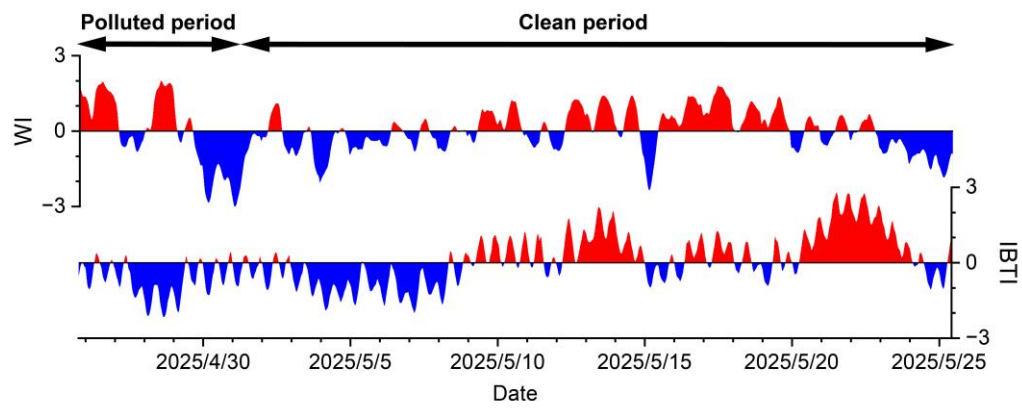
51

52 **Figure S5.** The westerlies index (WI) at QOMS and India-Burma Trough index (IBTI) during the study.

53
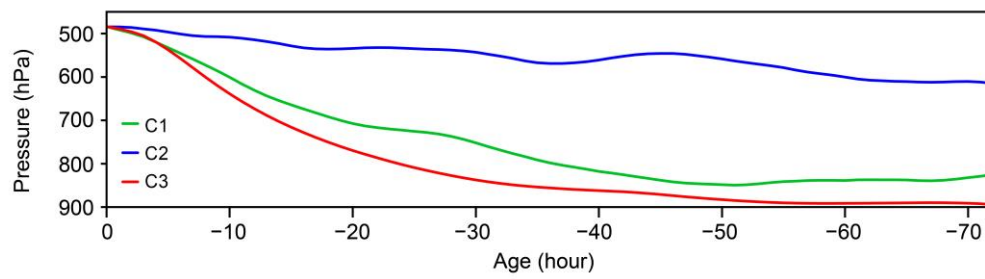
54

55 **Figure S6.** The atmospheric pressure of three backward-trajectory clusters.

56
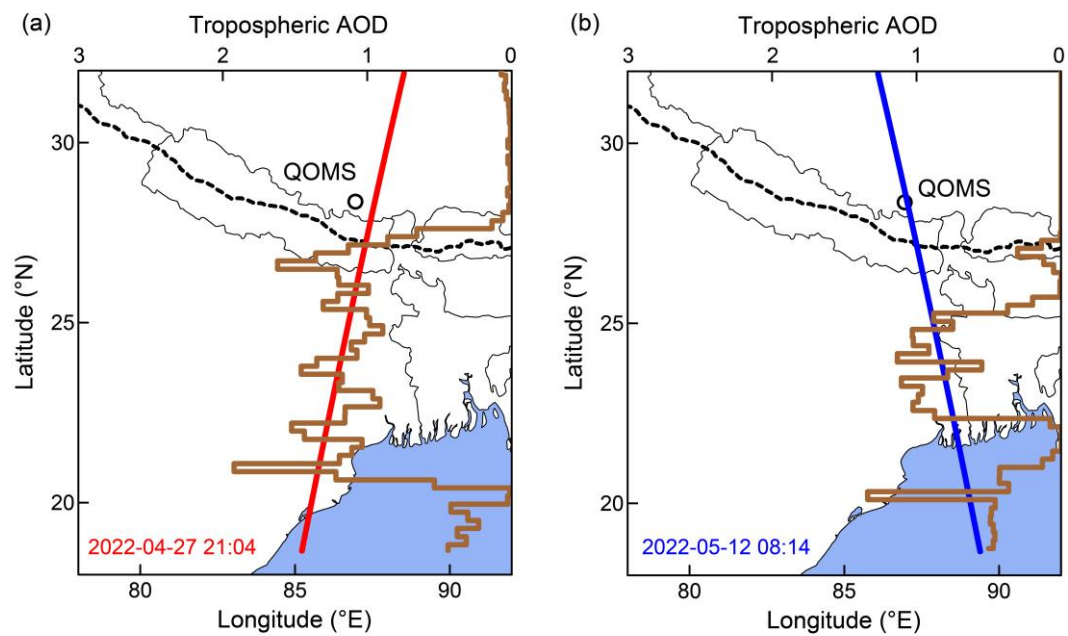
57

58 **Figure S7.** The Tropospheric AOD along the CALIPSO tracks on 27 April **(a)** and 12 May 2022 **(b)**. Dashed black lines
59 represent Tibetan Plateau boundary.

60
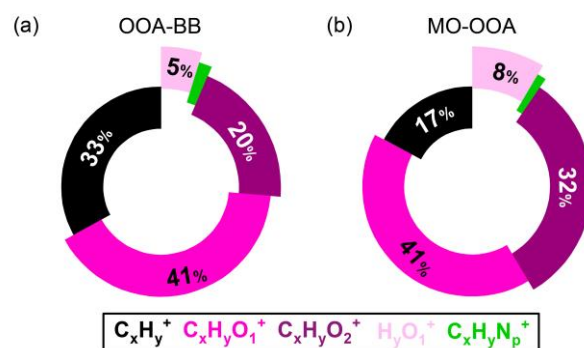
61

62 **Figure S8.** Five ion categories to OOA-BB **(a)** and MO-OOA **(b)** for the entire study.

63

64
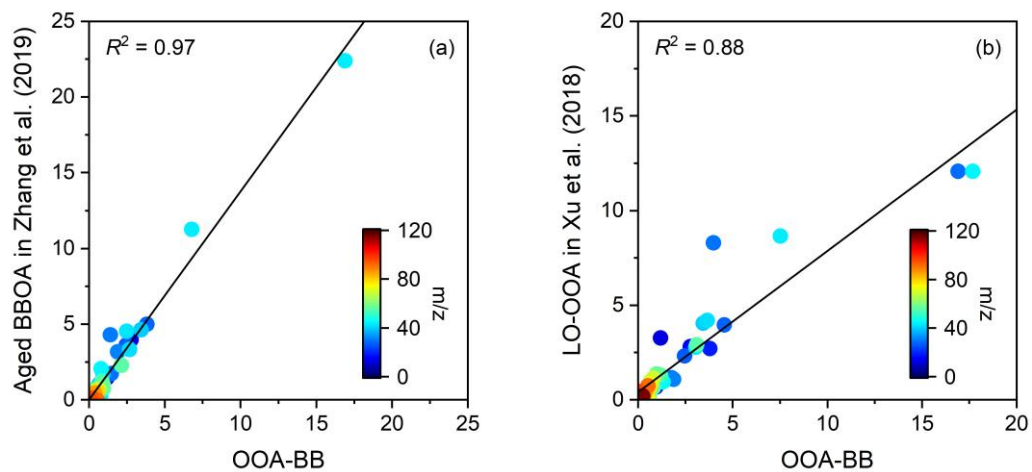
Figure S9. Comparisons between the OOA-BB HRMS identified in this study and HRMS determined from Zhang et al. (2019) and Xu et al. (2018).

67
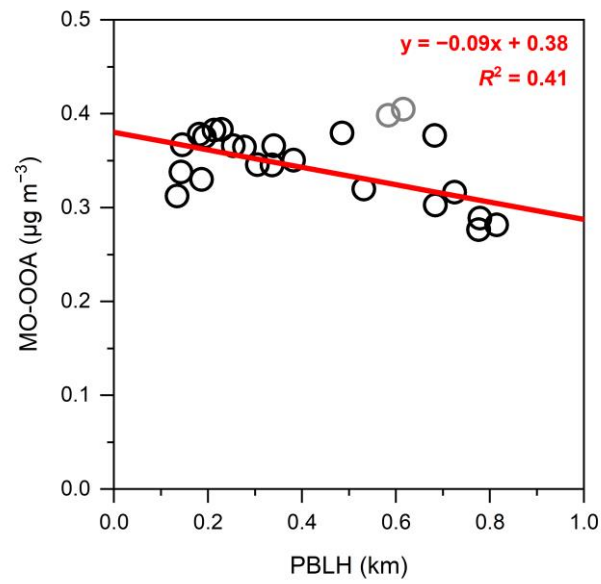
68

69 **Figure S10.** MO-OOA concentration as a function of ABLH. The grey circles are outliers (absolute value of studentized
70 residuals > 2), which might be due to the impact of other processes rather than ABLH.

71

72 **Table S1.** Pearson correlation coefficients and linear regression slopes for OOA factors with O_x, SOR, ALWC, and NOR grouped by daytime (solar radiation > 0) and nighttime (solar
73 radiation = 0). "ns" represents the slope is not significantly non-zero at $p = 0.05$.

	Day			Night		
	ΣOOA	MO-OOA	OOA-BB	ΣOOA	MO-OOA	OOA-BB
O_x	$r = 0.58$ slope = 0.050 ± 0.005	$r = 0.65$ slope = 0.025 ± 0.002	$r = 0.50$ slope = 0.025 ± 0.003	$r = 0.72$ slope = 0.042 ± 0.003	$r = 0.69$ slope = 0.020 ± 0.001	$r = 0.68$ slope = 0.023 ± 0.002
SOR	$r = 0.66$ slope = 24 ± 2.0	$r = 0.67$ slope = 11 ± 0.9	$r = 0.62$ slope = 13 ± 1.3	$r = 0.74$ slope = 15 ± 0.9	$r = 0.80$ slope = 7.9 ± 0.4	$r = 0.62$ slope = 7.2 ± 0.6
NOR	$r = 0.60$ slope = 8.7 ± 0.8	$r = 0.61$ slope = 3.9 ± 0.4	$r = 0.56$ slope = 4.8 ± 0.5	$r = 0.86$ slope = 11 ± 0.4	$r = 0.80$ slope = 5.4 ± 0.2	$r = 0.79$ slope = 5.8 ± 0.3
ALWC	$r = 0.31$ slope = 0.52 ± 0.17	$r = 0.12$ slope = 0.08 ± 0.08^{ns}	$r = 0.42$ slope = 0.43 ± 0.10	$r = 0.77$ slope = 0.84 ± 0.06	$r = 0.80$ slope = 0.37 ± 0.02	$r = 0.71$ slope = 0.47 ± 0.04

74

References

Chen, Y., Guo, H., Nah, T., Tanner, D.J., Sullivan, A.P., Takeuchi, M., Gao, Z., Vasilakos, P., Russell, A.G., Baumann, K., Huey, L.G., Weber, R.J., and Ng, N.L.: Low-Molecular-Weight Carboxylic Acids in the Southeastern US: Formation, Partitioning, and Implications for Organic Aerosol Aging, Environ. Sci. Technol., 55, 6688–6699, https://doi.org/10.1021/acs.est.1c01413, 2021.

Schueneman, M.K., Nault, B.A., Campuzano-Jost, P., Jo, D.S., Day, D.A., Schroder, J.C., Palm, B.B., Hodzic, A., Dibb, J.E., and Jimenez, J.L.: Aerosol pH indicator and organosulfate detectability from aerosol mass spectrometry measurements, Atmos. Meas. Tech., 14, 2237–2260, https://doi.org/10.5194/amt-14-2237-2021, 2021.

Xu, J., Zhang, Q., Shi, J., Ge, X., Xie, C., Wang, J., Kang, S., Zhang, R., and Wang, Y.: Chemical characteristics of submicron particles at the central Tibetan Plateau: insights from aerosol mass spectrometry, Atmos. Chem. Phys., 18, 427–443, https://doi.org/10.5194/acp-18-427-2018, 2018.

Zhang, Q., Jimenez, J.L., Worsnop, D.R., and Canagaratna, M.: A case study of urban particle acidity and its influence on secondary organic aerosol, Environ. Sci. Technol., 41, 3213–3219, https://doi.org/10.1021/es061812j, 2007.

Zhang, X., Xu, J., Kang, S., Zhang, Q., and Sun, J.: Chemical characterization and sources of submicron aerosols in the northeastern Qinghai–Tibet Plateau: insights from high-resolution mass spectrometry, Atmos. Chem. Phys., 19, 7897–7911, https://doi.org/10.5194/acp-19-7897-2019, 2019.